Hardness analysis of cubic metal mononitrides from first principles

B. D. Fulcher,[1] X. Y. Cui,[1,2] B. Delley,[3] and C. Stampfl[1]
[1]*School of Physics, The University of Sydney, Sydney 2006, NSW Australia*
[2]*Australian Centre for Microscopy & Microanalysis, The University of Sydney, New South Wales, 2006, Australia*
[3]*Paul Scherrer Institut WHGA/123 CH-5232 Villigen PSI, Switzerland*
(Received 15 November 2011; revised manuscript received 18 January 2012; published 17 May 2012)

Density functional theory calculations are performed to evaluate the hardness of various cubic metal nitrides: rocksalt TiN, VN, ZrN, NbN, AlN, and SiN; zincblende AlN and BN; and diamond C for comparison. The isotropic elastic stiffness constants c_{ij}, bulk modulus K, shear modulus G, Young's modulus E, and isotropic Poisson's ratio $\bar{\nu}$ are calculated. From simulated uniaxial stress-strain curves, ideal strength values $\sigma_{\max}$ in the [100], [110], and [111] directions are also evaluated for all systems. In particular, rocksalt AlN is found to possess both high elastic moduli and ideal strength. These quantities are then compared for correlations with existing experimental Vicker's hardness data. The bulk modulus is found to be a poor indicator of hardness, while E, G, $1/\bar{\nu}$, and $\sigma_{\max}$ all exhibit stronger correlations. With a view to circumvent the need to run computationally expensive relaxation steps, different methodologies for approximating uniaxial stress-strain curves are introduced. Utilizing the anisotropic Poisson's ratio to approximate the relaxed transverse lattice parameters at a given axial strain is a good approximation to stress-strain curves, and the ideal strengths obtained in this way exhibit strong correlations to experimental Vicker's hardness values.

DOI: 10.1103/PhysRevB.85.184106 PACS number(s): 71.23.−k, 71.55.Eq, 75.50.−y, 85.75.−d

I. INTRODUCTION

Hardness describes the extent to which a material resists elastic and plastic deformation, being defined experimentally by the ratio of the load to the area of impression when an indenter is forced onto a material surface.[1] Different hardness scales, including Brinell, Rockwell, Vickers, and Knoop, refer to particular characteristics of the indenter, and yield experimental hardness values that can vary by more than 10% for a given sample.[2] Since the experimental hardness test involves a complex mixture of both elastic (reversible) and plastic (permanent, bond-breaking) deformations, its quantitative modeling from *ab initio* calculation poses a particular challenge.

A material's hardness has commonly been estimated by considering equilibrium elastic quantities such as the bulk modulus K, shear modulus G, Young's modulus E, and Poisson's ratio ν. These mechanical quantities characterize the response of materials to small deformations, that is, in the small strain limit, where the stress-strain relationship is approximately linear. For some cases, equilibrium elastic properties do not provide a reliable indication of material hardness because the hardness measurement involves a complex mixture of elastic and plastic deformations at high strain.[3–5] In particular, it has been shown that the bulk modulus does not correlate with hardness for some ionic and covalent materials.[1,2,6] While the shear modulus is a more reliable indicator of hardness,[2,6–8] the dependence is not unequivocal and monotonic.[9]

Beyond the elastic regime, the use of the ideal strength of a material as an indicator of hardness has attracted increased attention recently.[10–16] Simulating an infinite, perfect crystal subjected to increasing strain, the stress-strain curve captures this deformation process: initially at equilibrium, straining through the elastic regime, and finally the point of structural instability. This critical point, which corresponds to a maximum in the stress-strain curve, is termed the *ideal strength*, $\sigma_{\max}$. As defects usually contribute to losses in strength, the theoretical ideal strength represents an upper bound on the stress a physical material can withstand.[10] The ideal strength is an inherent property of a crystal lattice and thus offers insight into the relationship between the intrinsic chemical bonding and symmetry of a crystal to its mechanical properties. $\sigma_{\max}$ is expected to be a better indicator of hardness than equilibrium elastic properties because it characterizes the material far from equilibrium, up to its theoretical breaking point.

Superhard materials exhibit a hardness greater than 40 GPa, and have wide applications as blades, grinding and polishing tools, and wear-resistant coatings.[17] As such, active research efforts are directed towards designing and fabricating superhard materials with desirable properties, such as low cost, chemical inertness, and thermal stability. Metal nitride systems possess desirable properties such as oxidation resistance and known relevance as potential superhard material components. For example, the refractory characteristics of TiN and ZrN have been widely applied as coatings to increase the wear resistance of cutting tools and as magnetic storage devices.[18–20] A new generation of coating development can be achieved through nanotechnology using metal nitrides: for example, the ternary Ti–Si–N system can form nanocomposites,[21] multilayers, and superlattices[21,22] with superhardening effects. Heterostructures such as TiN/VN, TiN/NbN,[23] and AlN/TiN[16] multilayered coatings can also possess greater hardness than single layers of the same materials. The transition metal nitrides are therefore an interesting and relevant test class of materials to focus upon. The rocksalt (*rs*) TiN, VN, ZrN, NbN, *rs*-AlN, and SiN, zincblende (*zb*) structures *zb*-AlN, *zb*-BN, and diamond structure *dia*-C are treated in this work. Note that we adopt a convention throughout the paper of only labeling systems that are *not* rocksalt structures (and *rs*-AlN to distinguish it from *zb*-AlN).

To our knowledge, a systematic comparison of elastic quantities, ideal strengths, and experimental hardness has not been reported and hence forms a core motivation for this work. Furthermore, despite intense research efforts into metal nitrides, a systematic theoretical study of their stress-strain

relationships and consequently their ideal strengths is lacking. In this paper we report *ab initio* calculations of elastic properties, including the stiffness constants c_{ij}, bulk modulus K, shear modulus G, Young's modulus E, isotropic Poisson's ratio $\overline{\nu}$, uniaxial stress-strain curves, and ideal strengths for all the above-mentioned systems. We calculate the Poisson's ratio and simulate stress-strain curves in each of the three primary [100], [110], and [111] directions. These calculated properties are compared to experimental Vicker's hardness measurements as a means of determining useful theoretical indicators. We also propose a method that uses the anisotropic Poisson's ratio to approximate the relaxed transverse lattice parameters at a given axial strain. This approach greatly reduces the computational cost of such calculations, and can produce reliable ideal strength values.

II. COMPUTATIONAL DETAILS

All calculations presented in this work are performed using density-functional theory (DFT) and the generalized gradient approximation (GGA)[24] for the exchange-correlation functional, as implemented in the all-electron periodic DMol^3 program.[25,26] The DMol^3 method employs fast converging three-dimensional numerical integrations to calculate the matrix elements occurring in the Ritz variational method. The wave functions are expanded in terms of a double-numeric quality localised basis set with polarization functions and an atomic real-space cutoff of 12–13 bohr for metal atoms and 7–8 bohr for N and C atoms.

For all the rocksalt, zincblende, and diamond structures, the Brillouin-zone integrations are performed using a large 12×12×12 Monkhorst-Pack grid for the unit cell, yielding 56 special **k** points in the irreducible part of the Brillouin zone. For the transformed unit cells used for calculating stress-strain curves, the grids are folded to obtain the same or similar sampling of reciprocal space. Except where stated otherwise, full structural relaxation, including lattice constants and internal atomic parameters, are performed for all systems.

The equilibrium lattice constants are obtained by calculating the total energy at a range of volumes and then fitting the obtained curve to the Murnaghan equation of state.[27] The elastic constants are derived by applying a set of homogeneous deformations and calculating from the second derivative of the total energy as a function of volume, tetragonal, and trigonal lattice distortions around the equilibrium structures, as implemented in DMol^3 code.

Submitting a material to uniaxial strain, a transformed unit cell is required in which one axis corresponds to the required strain direction. Strain in that crystallographic direction can then be simulated by varying the appropriate lattice parameter in that direction. The appropriate unit cells for modeling applied stain in the three primary directions: [100], [110], and [111], are shown in Fig. 1. For a rocksalt, zincblende, or diamond unit cell with an equilibrium lattice constant a_0, the unstrained cell used to model strain in the [100] direction is cubic, with lattice constants (a_0, a_0, a_0); in the [110] direction it is orthorhombic, with lattice constants ($a_0/\sqrt{2}$, $a_0/\sqrt{2}$, a_0); and in the [111] direction it is hexagonal with lattice constants ($a_0/\sqrt{2}$, $a_0/\sqrt{2}$, $\sqrt{3}a_0$). The atoms in rocksalt cells are octahedrally coordinated while in the zincblende (or diamond) cells are tetrahedrally coordinated.

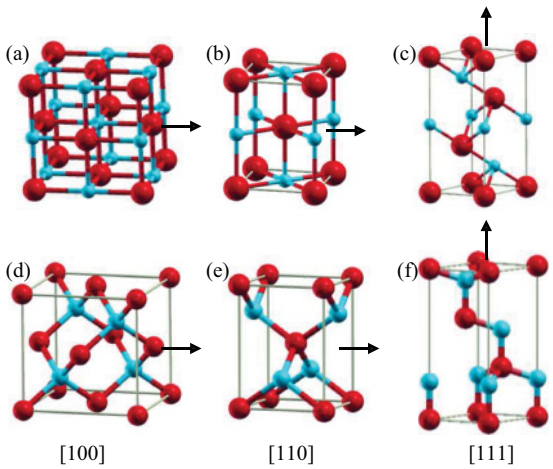

FIG. 1. (Color online) The transformed unit cells used to model strain in the [100], [110], and [111] directions for (a)–(c) rocksalt and (d)–(f) zincblende/diamond structures. Distortion of these cells in the direction of the arrow simulates strain in the required direction. The large dark and small pale spheres represent cations and anions, respectively.

III. RESULTS

A. Elastic properties

A generalized version of Hooke's law assumes that at each point in a medium the strains are linear functions of the stresses, and can be written as $\epsilon_i = s_{ij}\sigma_j$ or $\sigma_i = c_{ij}\epsilon_j$, where $i,j = 1,2,\ldots,6$, s_{ij} are the elastic compliances, and c_{ij} are the elastic stiffnesses.[28] The calculated stiffnesses c_{ij} can be used to map to the corresponding compliances s_{ij} by inverting the relations given in Ref. 28, as follows:

$$s_{11} = \frac{c_{11}+c_{12}}{c_{11}^2 + c_{11}c_{12} - 2c_{12}^2}, \tag{1}$$

$$s_{12} = -\frac{c_{12}}{c_{11}^2 + c_{11}c_{12} - 2c_{12}^2}, \tag{2}$$

$$s_{44} = \frac{1}{c_{44}}. \tag{3}$$

The Poisson's ratio ν measures a material's tendency to react to applied strain by altering the lattice parameters transverse to the applied strain. It is given by

$$\nu = -\epsilon_{\mathrm{tr}}/\epsilon, \tag{4}$$

where ϵ and ϵ_{tr} are the axial and transverse strains, respectively. Expressions for the Poisson's ratio for cubic systems (averaged over transverse directions) in the [100], [110], and [111] directions have been determined by Wojciechowski[29]:

$$\nu_{[100]} = -\frac{s_{12}}{s_{11}}, \tag{5}$$

$$\nu_{[110]} = -\frac{s_{11}+2s_{12}-s_{44}/2}{s_{11}+2s_{12}+s_{44}}, \tag{6}$$

$$\nu_{[111]} = -\frac{s_{11}+3s_{12}-s_{44}/2}{2s_{11}+2s_{12}+s_{44}}. \tag{7}$$

The shear modulus in the Voigt approximation[30] is given by

$$G_V = \tfrac{1}{5}\,(c_{11} - c_{12} + 3c_{44})\,, \tag{8}$$

and in the Reuss approximation[31] by

$$G_R = \frac{5}{4(s_{11} - s_{12}) + 3s_{44}} = \frac{5c_{44}(c_{11} - c_{12})}{4c_{44} + 3(c_{11} - c_{12})}. \tag{9}$$

The Voigt and Reuss approximations represent upper and lower bounds for the stiffness matrix coefficients of a given composite. Taking the mean $G = (G_V + G_R)/2$ gives an approximate measure of the isotropic shear modulus.[32] For cubic systems, the isotropic bulk modulus K, which quantifies a material's resistance to volume compression, is equivalent under both approximations to

$$K = \tfrac{1}{3}\,(c_{11} + 2c_{12})\,. \tag{10}$$

Using these quantities, we can then determine the isotropic Young's modulus,

$$E = \frac{9KG}{3K + G}, \tag{11}$$

which encapsulates a material's resistance to linear compression, and the isotropic Poisson's ratio,

$$\overline{\nu} = \frac{3K - 2G}{2\,(3K + G)}. \tag{12}$$

We label the isotropic Poisson's ratio $\overline{\nu}$ to distinguish it from the general anisotropic Poisson's ratio ν and, specifically, $\nu_{[100]}$, $\nu_{[110]}$, and $\nu_{[111]}$.

The calculated equilibrium lattice parameters a_0, stiffness constants c_{11}, c_{12}, and c_{44}, and the other isotropic elastic quantities are given in Table I. Since there is a vast amount of existing data for the lattice constants and elastic constants in the literature, we refer to some theoretical[34,35] and experimental results for comparison: for TiN,[36–40] ZrN,[19,38,39,41] NbN,[19,39] VN,[37–40] *zb*-AlN,[42,43] *zb*-BN,[43,44] and *dia*-C[1] (and references therein). In general, our calculated lattice constants and elastic constants are in good agreement with available data, except for ZrN from Ref. 41, in which the calculated elastic constants are 304, 114, and 511 GPa for c_{11}, c_{12}, and c_{44}, respectively (our values, cf. Table I, are 528, 95, and 126 GPa) . We point out that the data in Ref. 41 are self-contradictory; their elastic constants will lead to shear modulus $G_V = 344.6$ GPa and $G_R = 185.7$ GPa, not 261 and 251 GPa as reported in the same paper. Our results are in a much better agreement with the values reported in Refs. 19, 35, and 39. The calculated tendency of the elastic constants of NbN ($c_{11} > c_{12} > c_{44}$) and ZrN ($c_{11} > c_{44} > c_{12}$) is in accordance with the neutron scattering measurements, and the values are in better agreement with experiments than DFT-pseudopotential calculations[19] for both ZrN and NbN. In addition, the presently calculated $\nu_{[100]}$ values for NbN (0.175) and ZrN (0.152) exhibit good agreement with experimental values (0.18 and 0.16, respectively).[19]

As expected, the isotropic Poisson's ratio is approximately an average of the Poisson's ratio in each of the three primary directions, that is, $\overline{\nu} \approx (\nu_{[100]} + \nu_{[110]} + \nu_{[111]})/3$. We also note that the values of different elastic properties are not consistently ordered, suggesting different degree of correlation to hardness. For example, while K (isotropic bulk modulus) of TiN is less than that of VN and NbN, G (shear modulus), E (Young's modulus), and H (Vicker's hardness) are all greater. Interestingly, NbN exhibits a large value of c_{11} but a small value of c_{44} and, consequently, low G, E, and H despite exhibiting a relatively large K. The artificial rocksalt SiN has a low K, E, and G, and high $\overline{\nu}$, consistently indicating that it is a material with low hardness. By contrast, it is predicted that *rs*-AlN, which has a much smaller lattice constant than *zb*-AlN, may possess high hardness as it has a small calculated $\overline{\nu}$, large stiffness constants, particularly c_{12} and c_{44}, and large G and E, albeit a rather modest K value. It is worth noting that our elastic properties of *rs*-AlN are in excellent agreement with those reported recently in Ref. 35, who noted the particularly high value of c_{44} compared to the group IVB and VB transition metal nitrides.

B. Uniaxial stress-strain curves and ideal strength

Uniaxial strain is defined by

$$\epsilon = \frac{a - a_0'}{a_0'}, \tag{13}$$

where a and a_0' are the stretched and equilibrium transformed lattice parameters, respectively, in the direction of strain. Note

TABLE I. Calculated equilibrium lattice parameters a_0, stiffness constants c_{11}, c_{12}, c_{44}, Poisson's ratios in the three primary directions $\nu_{[100]}$, $\nu_{[110]}$, $\nu_{[111]}$, the isotropic Poisson's ratio $\overline{\nu}$, bulk modulus K, Young's modulus E, shear modulus G, and, where available, experimental Vicker's hardness values H.

	a_0 (Å)	c_{11}	c_{12}	c_{44}	$\nu_{[100]}$	$\nu_{[110]}$	$\nu_{[111]}$	$\overline{\nu}$	K (GPa)	E (GPa)	G (GPa)	H (GPa)
SiN	4.28	207	150	71	0.420	0.361	0.315	0.367	169	135	49	
ZrN	4.62	528	95	126	0.152	0.254	0.275	0.231	239	386	157	18 ± 1[a]
NbN	4.45	630	134	85	0.175	0.348	0.371	0.307	299	346	133	14 ± 1[a]
VN	4.13	591	159	137	0.212	0.287	0.304	0.270	303	417	164	15 ± 1[a]
TiN	4.26	531	118	166	0.182	0.222	0.233	0.213	256	440	181	18 ± 2[a]
AlN	4.07	434	159	315	0.269	0.140	0.058	0.154	251	521	226	
zb-AlN	4.40	309	162	192	0.344	0.233	0.151	0.243	211	325	131	18[b]
zb-BN	3.63	800	170	450	0.175	0.106	0.076	0.118	380	872	390	63 ± 5[a]
dia-C	3.57	1036	113	541	0.099	0.063	0.050	0.070	421	1086	508	96 ± 5[a]

[a]Reference 7.
[b]Reference 33.

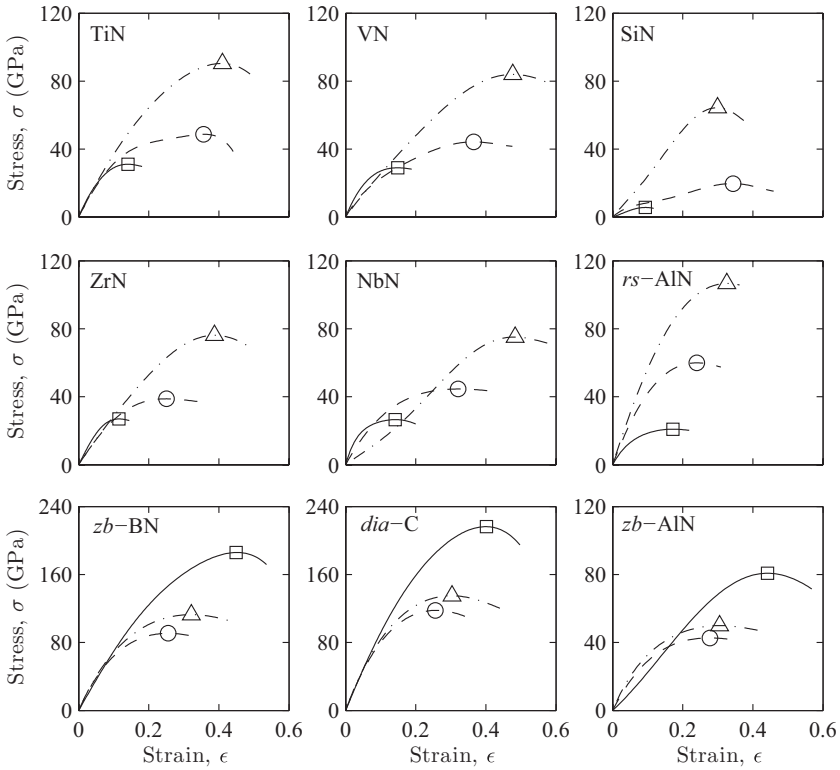

FIG. 2. Uniaxial "relaxed" stress-strain curves in the [100] direction: solid line/squares; the [110] direction: dashed line/circles; and the [111] direction: dot-dashed line/triangles. Local maximums correspond to points of critical strain and ideal strength, $(\epsilon_c,\sigma_{\max})$, and are labeled in each case by the relevant symbol (a square, circle, or triangle). Points on the stress-strain curves are not raw data points, but are fitted from the energy-strain data and therefore suppressed from these plots for clarity. Note the increased vertical scale for the *zb*-BN and *dia*-C structures.

a_0' corresponds to a_0, $a_0/\sqrt{2}$, and $\sqrt{3}a_0$ for strains in the [100], [110], and [111] directions, respectively (where a_0 is the lattice constant of the equilibrium, untransformed cubic unit cell). Stress is defined as

$$\sigma = \frac{1}{V_0}\frac{dU}{d\epsilon}, \tag{14}$$

where V_0 is the equilibrium volume and U is the total energy of the system.

Stress-strain curves in a given crystallographic direction are modeled by calculating the total energy at a series of incremental strains. In this study we consider the strain in the [100], [110], and [111] directions for the cubic structures, as shown in Fig. 1. For each system, and in each direction, we calculate the total energy for at least five different strain values, ensuring that a sufficient range has been explored to include the maximum of the stress-strain curve. The transverse lattice parameters are relaxed to minimize the total energy at each strain increment. To the total energy versus applied strain values, we fit a fifth order polynomial, under the constraint that the first order coefficient be zero. From the $U(\epsilon)$ fit described above, $dU/d\epsilon(\epsilon)$ is determined analytically, where points on the stress-strain curve are calculated from Eq. (14).

The calculated uniaxial stress-strain curves for all systems are shown in Fig. 2. Because the transverse lattice parameters were relaxed at each strain increment, we label this method "relaxed," in contrast to other approximations that will be explored in Sec. III C below. We derive two summary statistics from each of these curves: the ideal strength $\sigma_{\max}$ and the *critical strain* ϵ_c, which are the stress and strain values at the local maximum, respectively. Intuitively, ϵ_c corresponds to the minimum strain required to plastically deform an infinite defect-free crystal. For all systems in each of the three directions, these values are presented in Table II in the columns labeled relaxed. A material with high hardness is expected to have large $\sigma_{\max}$ and ϵ_c values, and preferably in all directions. The stress-strain curve also gives a visual indication of the (anisotropic) Young's modulus E, which is the gradient of the stress-strain curve in the low strain limit ($\epsilon \to 0$).

The stress-strain relationships studied here are clearly anisotropic, which is consistent with the results of other *ab initio* studies, including those of rocksalt AlN and TiN,[16] and carbon networks.[45,46] For the rocksalt structures, the observed trend $\sigma_{[111]} > \sigma_{[110]} > \sigma_{[100]}$ can be understood in terms of the bonding arrangement. In strong directions there exists an angle between the bonding direction and that of the applied strain such that additional work is required to induce angular distortions.[46] While strain applied in the [110] and [111] directions stretch the metal–N bonds at an angle to the bond direction, [100] strain results in stretching directly along the metal–N bonds, maximizing the work put into bond breaking. The ideal strength $\sigma_{[100]}$ is consequently minimal for the rocksalt structures. For the [111] direction, metal–N bonds are at the greatest angle to the direction of applied strain; [110] is an intermediate case. Thus we have the observed trend $\sigma_{[111]} > \sigma_{[110]} > \sigma_{[100]}$ for the rocksalt structures. The anisotropy of the zincblende/diamond structures $\sigma_{[100]} > \sigma_{[111]} > \sigma_{[110]}$ can be explained using similar arguments. Since under uniform distortion a crystal breaks at the strain threshold of its weakest direction, the large differences between ideal strength values along different crystallographic directions are important. If a crystalline material is grown preferentially on a substrate in the strong strength direction, there should be a substantial increase in strength in this direction over that of the bulk sample.

We note the ideal cleavage strength values for TiN and VN in Ref. 37 are of the same trend as, but systematically

TABLE II. Ideal strengths $\sigma_{\max}$ (upper rows, GPa), and corresponding critical strains ϵ_c (lower rows, in parentheses), of all systems obtained from the stress-strain curves in each of the directions [100], [110], and [111]. Three methods are shown, using the anisotropic ν (Poisson's ratio), performing transverse relaxation at each strain increment (relaxed), and leaving the transverse lattice constants fixed at their equilibrium values (unrelaxed).

	$\sigma_{\max}$ (ϵ_c) Poisson's ratio			$\sigma_{\max}$ (ϵ_c) Relaxed			$\sigma_{\max}$ (ϵ_c) Unrelaxed		
	[100]	[110]	[111]	[100]	[110]	[111]	[100]	[110]	[111]
SiN	5	18	60	5	19	64	18	40	65
	(0.08)	(0.28)	(0.34)	(0.10)	(0.36)	(0.33)	(0.19)	(0.33)	(0.37)
ZrN	27	41	78	27	39	76	31	48	75
	(0.13)	(0.33)	(0.39)	(0.13)	(0.27)	(0.40)	(0.18)	(0.29)	(0.40)
NbN	28	50	84	27	36	76	34	46	76
	(0.13)	(0.57)	(0.50)	(0.12)	(0.44)	(0.50)	(0.18)	(0.34)	(0.47)
VN	30	47	85	29	44	84	36	56	89
	(0.16)	(0.43)	(0.49)	(0.14)	(0.39)	(0.49)	(0.19)	(0.35)	(0.50)
TiN	31	50	90	31	47	90	35	57	92
	(0.15)	(0.34)	(0.39)	(0.14)	(0.31)	(0.41)	(0.19)	(0.33)	(0.43)
AlN	23	60	107	21	60	107	29	66	106
	(0.19)	(0.29)	(0.31)	(0.16)	(0.25)	(0.33)	(0.21)	(0.30)	(0.32)
zb-AlN	85	45	51	81	43	50	79	47	51
	(0.43)	(0.27)	(0.29)	(0.44)	(0.27)	(0.28)	(0.47)	(0.30)	(0.38)
zb-BN	182	92	113	185	92	113	184	98	112
	(0.41)	(0.26)	(0.31)	(0.46)	(0.25)	(0.31)	(0.45)	(0.31)	(0.33)
dia-C	209	119	135	215	119	134	214	122	135
	(0.36)	(0.26)	(0.30)	(0.40)	(0.26)	(0.30)	(0.40)	(0.30)	(0.30)

lower (by 10%–15%), than the ideal strength values reported here, indicating that TiN and VN tend to fail by brittle cleavage. Consistent with its high elastic constants, it is important to notice the remarkable calculated ideal strength of *rs*-AlN, which is significantly higher than that of *zb*-AlN. By calculating the phonon density-of-states at the equilibrium and understrain structures, for different strain directions, we confirm that there is no imaginary phonon frequency, and thus no mechanical instability of the studied *rs*-AlN configurations. The octahedrally coordinated *rs*-AlN is isoelectronic to both BN and diamond, the latter two being the two hardest known bulk materials with tetrahedrally coordinated structure. AlN ordinarily crystallizes in the wurtzite (*wz*) structure, but can also form a zincblende structure with a similar (slightly less favorable) energy.[47] *rs*-AlN has a notably smaller calculated lattice constant compared to the *zb* phase, namely 4.07 Å versus 4.40 Å. The calculated value of 4.07 Å is in excellent agreement with other *ab initio* results, for example, 4.049 Å,[35] and with experiment 4.08 ± 0.02 Å quoted in Ref. 35. *rs*-AlN also has a significantly higher formation energy (by 10.5 eV/formular unit) compared to *zb*-AlN. Nevertheless, *rs*-AlN layers have been epitaxially grown on VN[48] and TiN[49] substrates as superlattices, where a hardness enhancement has been reported. Beyond a certain critical thickness of AlN, a phase transformation occurs in which AlN changes to the energetically preferred wurtzite structure, concomitant with a lower hardness.[50] The present theoretical results for high ideal strength and high elastic moduli, together with those in Ref. 35, suggest that these characteristics of *rs*-AlN may contribute to the measured hardness enhancement of VN/AlN[48] and TiN/AlN[49] superlattices, in addition to affording the formation of semicoherent TiN/AlN interfaces, as discussed in Ref. 16. Indeed, we also calculated the elastic constants for *wz*-AlN, and the obtained values are 379, 122, 97, 362, and 119 GPa for c_{11}, c_{12}, c_{13}, c_{33}, and c_{44}, respectively. The derived bulk modulus, Young's modulus, and shear modulus for *wz*-AlN are 194, 357, and 149 GPa, respectively, consistently lower than those of *rs*-AlN, namely 251, 521, and 226 GPa.

C. Methodological approximations

The relaxed method for calculating stress-strain curves, described above, is computationally expensive, mainly due to the task of minimizing the transverse lattice parameters at each strain increment. As such, we propose that this process can be simplified by exploiting the anisotropic Poisson's ratio. For conventional materials, the Poisson's ratio values lie within the range $0 \leqslant \nu \leqslant 0.5$. At one extreme, taking $\nu = 0$, implies that $\epsilon_{\rm tr} = 0$ and transverse lattice parameters remain at their equilibrium values, independent of strain. This approach, which we term the "unrelaxed" method, consistently overestimates the unit cell volume relative to letting the transverse lattice parameters relax to their equilibrium values under tensile strain. At the other extreme, with $\nu = 0.5$, transverse lattice parameters adjust so as to maintain the equilibrium volume V_0, consistently underestimating the relaxed unit cell volume under tensile strain. We find that this "fixed volume" method produces large differences in energy compared to the fully relaxed case for the systems studied here and therefore yields dramatically different stress-strain curves. Of course, one can also calculate the actual Poisson's ratio of a material in a given strain direction and use this to predict the transverse lattice constants at each strain increment. This approach, which we term the "Poisson's ratio" approximation to calculating stress-strain curves, is detailed below.

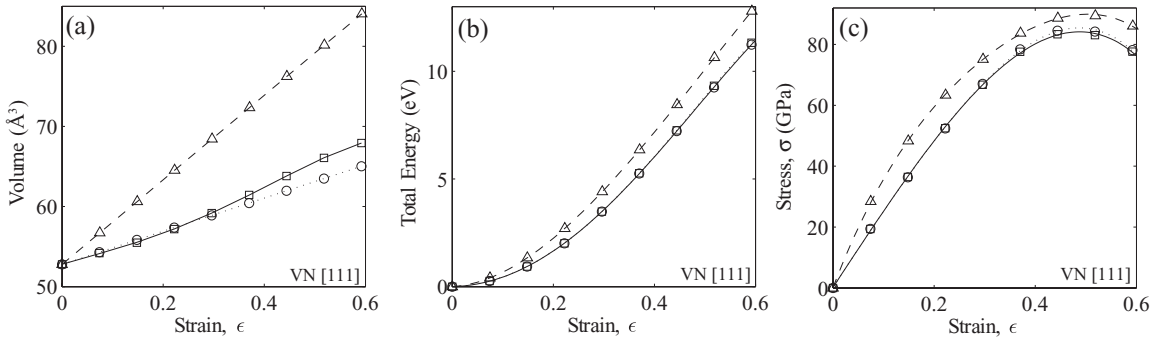

FIG. 3. Comparison of methodologies for obtaining stress-strain curves. (a) Unit cell volume, (b) total energy (relative to equilibrium), and (c) stress as a function of strain for VN in the [111] direction using the unrelaxed (triangle/dashed line) and Poisson's ratio (circle/dotted line) approximations to the fully relaxed (square/solid line) method.

Using the definitions for ϵ [Eq. (13)] and ν [Eq. (4)], the volume of an orthorhombic unit cell, corresponding to [100] and [110] directions, is $V = a_x a_y a_z$, and that of a hexagonal unit cell, corresponding to the [111] direction, is $V = a_x a_y a_z \sqrt{3}/2$, where a_x, a_y, a_z are the lattice parameters of the equilibrium, untransformed unit cell (cf. Fig. 1). Both of these expressions can be written as a function of strain as

$$V = V_0(1+\epsilon_{\rm tr})(1+\epsilon_{\rm tr})(1+\epsilon) = V_0(1-\nu\epsilon)^2(1+\epsilon). \tag{15}$$

Differentiating, we have

$$\frac{dV}{d\epsilon} = V_0(1-\nu\epsilon)(1-2\nu-3\nu\epsilon), \tag{16}$$

where V_0 is the equilibrium volume and ν is the anisotropic Poisson's ratio in the direction of strain. In the small strain limit, $\epsilon \to 0$, we evaluate Eq. (16) and integrate, yielding

$$V = V_0\left[1+\epsilon\,(1-2\nu)\right]. \tag{17}$$

Since $V = V_0(1+\epsilon_{\rm tr})^2(1+\epsilon)$, Eq. (17) can be written as

$$(1+\epsilon_{\rm tr})^2 = \frac{1+\epsilon(1-2\nu)}{1+\epsilon}. \tag{18}$$

Therefore, since $a_{\rm tr}/a_0' = 1+\epsilon_{\rm tr}$, the transverse lattice constants are given by a strain-dependent factor of their equilibrium value a_0' according to

$$a_{\rm tr}(\epsilon;\nu) = a_0'\sqrt{\frac{1+\epsilon(1-2\nu)}{1+\epsilon}}. \tag{19}$$

Therefore, assuming a linear variation of volume with strain, the anisotropic Poisson's ratio ν of a material in a given crystallographic direction can be used to approximate the relaxed transverse lattice constants $a_{\rm tr}$ as a function of the uniaxial strain ϵ. Instead of explicitly optimizing over the transverse lattice parameters at each strain increment, their relaxed values are predicted using the relevant (anisotropic) Poisson's ratio.

The performance of these two approximations relative to the fully relaxed method is illustrated in Fig. 3, using VN in the [111] direction as an example. The volume-strain relationship is shown in Fig. 3(a); in this case the Poisson's ratio method gives closer agreement to the relaxed relationship compared to the unrelaxed method, which consistently overestimates the unit cell volume. The total energy and stress versus strain curves are shown in Figs. 3(b) and 3(c), respectively. Despite overestimating the unit cell volume, the unrelaxed method produces a reasonable approximation to the fully relaxed stress-strain curve, however the Poisson's ratio method reproduces the relaxed results almost exactly. The values of the predicted ideal strength $\sigma_{\rm max}$ and corresponding critical strain ϵ_c for the three approaches, relaxed, unrelaxed, and Poisson's ratio for all systems are in Table II.

In Fig. 4 we further plot percentage deviations from $\sigma_{\rm max}$ values calculated using unrelaxed and Poisson's ratio methods relative to that obtained by the relaxed method. Figure 4(a) compares the average ideal strength $\overline{\sigma_{\rm max}} = (\sigma_{[100]}+\sigma_{[110]}+\sigma_{[111]})/3$ for the two approximate methods, and Fig. 4(b) compares the minimum ideal strength $\min(\sigma_{\rm max}) = \min(\sigma_{[100]},\sigma_{[110]},\sigma_{[111]})$. In general, the Poisson's ratio method is shown to be an improvement over the unrelaxed method, with a mean deviation from $\overline{\sigma_{\rm max}}$ of 3% and from $\min(\sigma_{\rm max})$ of 2%. By contrast, the unrelaxed method has a mean deviation of 42% for $\overline{\sigma_{\rm max}}$ (or 17% excluding the SiN outlier), and 10.6% for $\min(\sigma_{\rm max})$. Comparing the ideal strength in the weakest direction, that is, $\min(\sigma_{\rm max})$ in Fig. 4(b), shows that the Poisson's ratio method is a significant improvement over the unrelaxed method, deviating from the relaxed values by no more than 5% (except for NbN).

D. Correlations with Vicker's hardness

For the studied cubic systems we analyzed proportional correlations between various equilibrium elastic quantities and ideal strengths with experimental Vicker's hardness, as shown in Fig. 5. Coefficients of determination R^2 are calculated for lines constrained to pass through the origin, as a means of comparing each elastic quantity as a proportional indicator of material hardness. The isotropic ideal strength $\overline{\sigma_{\rm max}}$ is approximated as the average of the ideal strengths in each of the [100], [110], and [111] directions.

As shown in Fig. 5(a), the bulk modulus K, despite being a conventional indicator of material hardness, is found to give the worst correlation with hardness. This finding is consistent with other studies.[2,6–8] And although other studies highlight a discrepancy,[3,51] we find a reasonable proportional correlation between Young's modulus E and Vicker's hardness H for

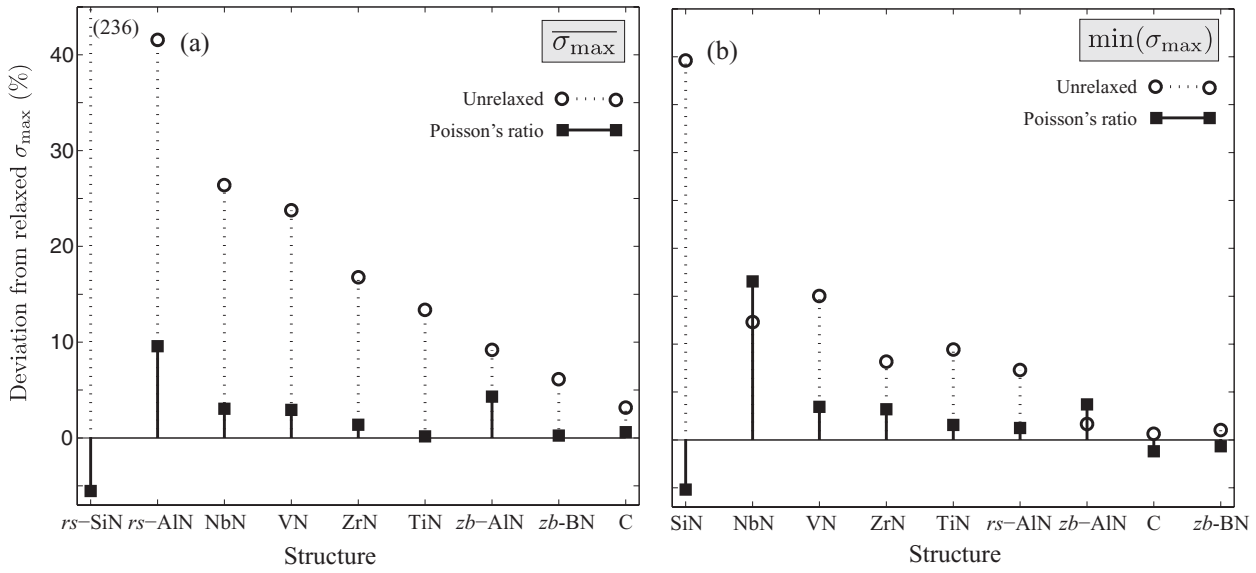

FIG. 4. Percentage deviations of $\sigma_{\max}$ obtained using the unrelaxed (circles, dotted line) and Poisson's ratio (squares, solid line) approximations to their fully relaxed values: (a) averaged over individual deviations in each of the [100], [110], and [111] directions, and (b) in the weakest principle direction (i.e., [100] for rocksalt structures, and [110] for zincblende/diamond structures). The raw data on which these graphs were obtained is in Table II. Vertical axis limits are chosen to reveal the variation across the systems, obscuring an outlying point for the unrelaxed method in (a), which overestimates $\overline{\sigma_{\max}}$ for SiN by 236% (as labeled).

the systems treated in this work [Fig. 5(b)]. The inverse of the isotropic Poisson's ratio $1/\overline{\nu}$ has not to our knowledge been used previously as an indicator of hardness, but for the systems studied here, it also yields a good proportional fit [Fig. 5(d)]. As shown in Figs. 5(e)–5(g), all three methods for obtaining ideal strengths show similar correlations to Vicker's hardness, with $R^2 > 0.97$. Thus, although the magnitudes of $\sigma_{\max}$ can vary between the methods for obtaining stress-strain curves (cf. Fig. 4 and Table II), for the systems studied here, these discrepancies do not significantly affect correlations to

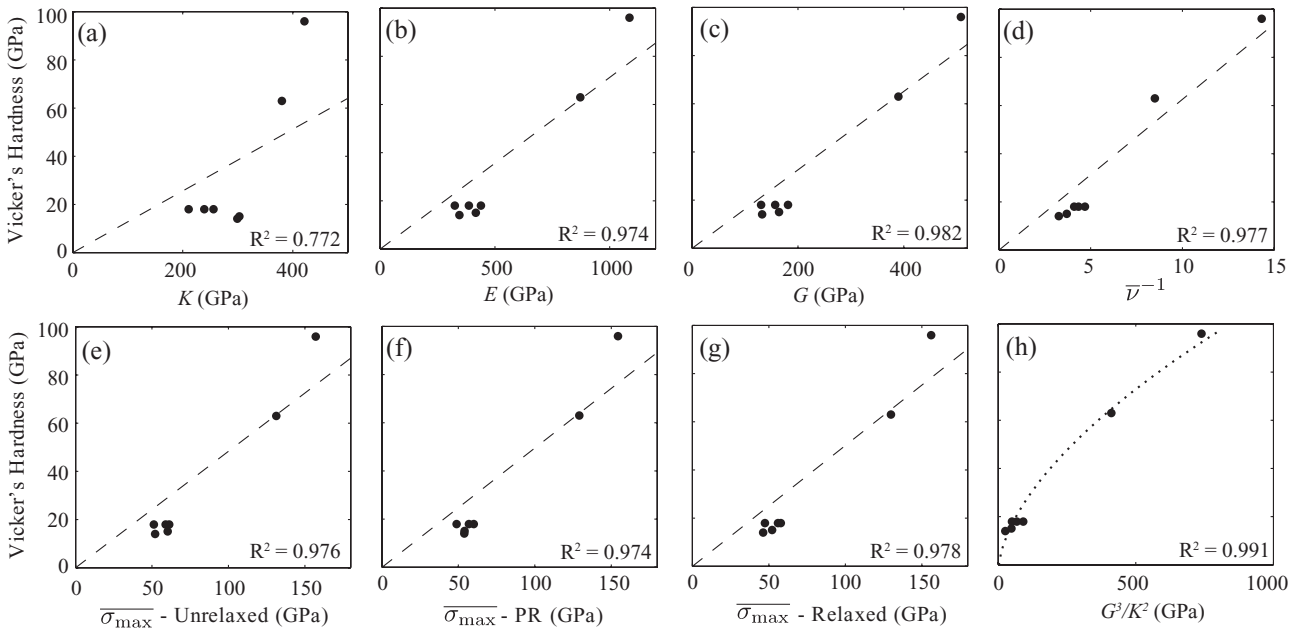

FIG. 5. Correlations of calculated mechanical properties with experimental Vicker's hardness H for all systems for which hardness data is available (cf. Table II): ZrN, NbN, VN, TiN, *zb*-AlN, *zb*-BN, and *dia*-C. We plot (a) bulk modulus K, (b) Young's modulus E, (c) shear modulus G, (d) the inverse of the isotropic Poisson's ratio $\overline{\nu}^{-1}$, and the ideal strength $\sigma_{\max}$ averaged over the [100], [110], and [111] directions $\overline{\sigma_{\max}}$ using the (e) unrelaxed, (f) Poisson's ratio, and (g) relaxed methods. In (h) we explore the relationship between Vicker's hardness and the quantity G^3/K^2 proposed in Ref. 52, including their hypothesized relationship $H = 2(G^3/K^2)^{0.585} - 3$ with a dotted line. Dashed lines represent linear fits to the data that are constrained to pass through the origin. Coefficients of determination R^2 are also included in each case.

Vicker's hardness. Also, due to the small sample size of the studied systems, we are unable to reliably distinguish between E, G, ν^{-1}, and $\sigma_{\max}$, all of which exhibit relatively strong correlations to H. For a wider range of more complicated materials, distinguishing the best indicators of hardness would be possible. Moreover, our proposed Poisson's ratio method is applicable to more complicated structures, yet its validity is to be explored.

Finally we investigated a recently proposed relationship between experimental Vicker's hardness and the bulk modulus $H = 2(G^3/K^2)^{0.585} - 3$, which was shown to hold for a large number of materials.[52] This relationship and the data for systems analyzed in this work are shown in Fig. 5(h). The obtained very high coefficients of determination $R^2 = 0.991$ is partially due to the inclusion of several systems (such as TiN, NbN, c-BN, and diamond) in the fitting in Ref. 52. Although we consider a relatively small number of systems in this work, the data are consistent with this proposed relationship.

IV. SUMMARY AND CONCLUSIONS

We have performed a systematic all-electron DFT study to investigate the hardness of various cubic metal mononitrides. The calculated elastic moduli are in good agreement with experimental and most theoretical data. Uniaxial stress-strain curves and ideal strength values were also presented. Significantly, rocksalt AlN exhibits much higher elastic moduli than the corresponding zincblende and wurtzite structures. To reduce the computational cost, different methodologies, including the unrelaxed, Poisson's ratio, and relaxed methods, for obtaining uniaxial stress-strain curves were developed and compared. In particular, a Poisson's ratio method that uses the anisotropic Poisson's ratio to approximate the relaxed transverse lattice parameters at a given axial strain, produces excellent agreement with the ideal strength values obtained via the relaxed method. For the systems considered here, the correlations between various theoretical mechanical properties and experimental Vicker's hardness values were investigated. The bulk modulus was found to be a poor indicator of hardness, while other quantities, particularly the shear modulus, the inverse of Poisson's ratio and the ideal strength, exhibited good proportional correlations. Future work, exploring the same quantities as in the present work, for a wider range of material systems would be valuable and may be able to distinguish which of these properties is the best indicator of hardness.

ACKNOWLEDGMENTS

We thank Shiqiang Hao for helpful discussion at the early stage of this work. We acknowledge the computing resources provided by the Australian National Computational Infrastructure (NCI) Facility and support from the Australian Research Council (ARC).

[1] V. Brazhkin, A. Lyapin, and R. Hemley, Philos. Mag. A **82**, 231 (2002).
[2] J. Haines, J. M. Leger, and G. Bocquillon, Ann. Rev. Mater. **31**, 1 (2001).
[3] F. Gao, J. He, E. Wu, S. Liu, D. Yu, D. Li, S. Zhang, and Y. Tian, Phys. Rev. Lett. **91**, 015502 (2003).
[4] F. Gao, Phys. Rev. B **73**, 132104 (2006).
[5] R. B. Kaner, J. J. Gilman, and S. H. Tolbert, Science **308**, 1268 (2005).
[6] J. M. Leger, P. Djemia, F. Ganot, J. Haines, A. S. Pereira, and J. A. H. da Jomada, Appl. Phys. Lett. **79**, 2169 (2001).
[7] D. M. Teter, MRS Bull. **23**, 22 (1998).
[8] H. Y. Chung, M. B. Weinberger, J. M. Yang, S. H. Tolbert, and R. B. Kaner, Appl. Phys. Lett. **92**, 261904 (2008).
[9] R. Yu and X. F. Zhang, Phys. Rev. B **72**, 054103 (2005).
[10] A. Kelly and N. H. Macmillan, *Strong Solids*, 3rd ed. (Clarendon, Oxford, 1986), Chap. 1.
[11] S. H. Jhi, S. G. Louie, M. L. Cohen, and J. Ihm, Phys. Rev. Lett. **86**, 3348 (2001).
[12] D. M. Clatterbuck, C. R. Krenn, M. L. Cohen, and J. W. Morris, Phys. Rev. Lett. **91**, 135501 (2003).
[13] M. Friak, M. Sob, and V. Vitek, Phys. Rev. B **68**, 184101 (2003).
[14] Y. Zhang, H. Sun, and C. Chen, Phys. Rev. B **73**, 144115 (2006).
[15] S. Hao, B. Delley, and C. Stampfl, Phys. Rev. B **74**, 035424 (2006).
[16] R. F. Zhang, S. H. Sheng, and S. Veprek, Appl. Phys. Lett. **91**, 031906 (2007).
[17] W. D. Sproul, Science **273**, 889 (1996).
[18] I. Milosev, H. H. Strehblow, and B. Navinsek, Thin Solid Films **303**, 246 (1997).
[19] X-J. Chen, V. V. Struzhkin, Z. Wu, M. Somayazulu, J. Qian, S. Kung, A. N. Christensen, Y. Zhao, R. E. Cohen, H-K. Mao, and R. J. Hemley, Proc. Nat. Acad. Sci. USA **102**, 3198 (2005).
[20] L. E. Toth, *Transition Metal Carbides and Nitrides* (Academic, New York, 1971).
[21] S. Veprek, M. G. J. Veprek-Heijman, P. Karvankova, and J. Prochazka, Thin Solid Films **476**, 1 (2005).
[22] H. Soderberg, M. Oden, J. M. Molina-Aldareguia, and L. Hultman, J. Appl. Phys. **97**, 114327 (2005).
[23] X. Chu, M. S. Wong, W. D. Sproul, S. L. Rohde, and S. A. Barnett, J. Vac. Sci. Technol. A **10**, 1604 (1992).
[24] J. P. Perdew, K. Burke, and M. Ernzerhof, Phys. Rev. Lett. **77**, 3865 (1996).
[25] B. Delley, J. Chem. Phys. **92**, 508 (1990).
[26] B. Delley, J. Chem. Phys. **113**, 7756 (2000).
[27] F. D. Murnaghan, Proc. Natl. Acad. Sci. USA **30**, 244 (1944).
[28] J. Nye, *Physical Properties of Crystals* (Oxford University Press, London, 1957).
[29] K. W. Wojciechowski, *Slow Dynamics in Complex Systems*, AIP Conf. Proc., edited by M. Tokuyama and I. Oppenheim, Vol. 708 (American Institute of Physics, New York, 2004), pp. 735–738.
[30] W. Voigt, *Lehrbuch der Kristallphysik* (Teubner, Leipzig, 1928).
[31] A. Reuss, Z. Angew. Math. Mech. **9**, 49 (1929).
[32] E. Schreiber, O. L. Anderson, and N. Soga, *Elastic Constants and Their Measurement* (McGraw-Hill, New York, 1973).
[33] I. Yonenaga, MRS Internet J. Nitride Semicond. Res. **7**, 6 (2002).
[34] C. Stampfl, W. Mannstadt, R. Asahi, and A. J. Freeman, Phys. Rev. B **63**, 155106 (2001).

[35]D. Holec, M. Friak, J. Neugebauer, and P. H. Mayrhofer, Phys. Rev. B **85**, 064101 (2012).
[36]R. Ahuja, O. Eriksson, J. M.Wills, and B. Johansson, Phys. Rev. B **53**, 3072 (1996).
[37]P. Lazar, J. Redinger, and R. Podloucky, Phys. Rev. B **76**, 174112 (2007).
[38]K. Chen and M. Bielawski, Surf. Coat. Technol. **203**, 598 (2008).
[39]M. G. Brik and C. G. Ma, Comput. Mater. Sci. **51**, 380 (2012).
[40]W. Wolf, R. Podloucky, T. Antretter, and F. D. Fisher, Philos. Mag. B **79**, 839 (1999).
[41]D. Cheng, S. Wang, and H. Ye, J. Alloys Compd. **377**, 221 (2004).
[42]M. B. Kanoun, S. Goumri-Said, A. E. Merad, G. Merad, J. Cobert, and H. Aourag, Semicond. Sci. Technol. **19**, 1220 (2004).
[43]K. Shimada, T. Sota, and K. Suzuki, J. Appl. Phys. **84**, 4951 (1998).
[44]Y. D. Guo, X. D. Yang, S. B. Li, X. S. Song, and X. L. Cheng, Diam. Relat. Mater. **17**, 1 (2008).
[45]X. Blase, P. Gillet, A. SanMiguel, and P. Melinon, Phys. Rev. Lett. **92**, 215505 (2004).
[46]R. H. Telling, C. J. Pickard, M. C. Payne, and J. E. Field, Phys. Rev. Lett. **84**, 5160 (2000).
[47]N. E. Christensen and I. Gorczyca, Phys. Rev. B **50**, 4397 (1994).
[48]G. Y. Li, J. J. Lao, J. W. Tian, Z. H. Han, and M. Y. Gu, J. Appl. Phys. **95**, 92 (2004).
[49]A. Madan, I. W. Kim, S. C. Cheng, P. Yashar, V. P. Dravid, and S. A. Barnett, Phys. Rev. Lett. **78**, 1743 (1997).
[50]I. W. Kim, Q. Li, L. D. Marks, and S. A. Barnett, Appl. Phys. Lett. **78**, 892 (2001).
[51]Y. Zhang, H. Sun, and C. Chen, Phys. Rev. Lett. **93**, 195504 (2004).
[52]X. Q. Chen, H. Y. Niu, D. Z. Li, and Y. Y. Li, Intermetallics **19**, 1275 (2011).